

Multistability in lossy power grids and oscillator networks

Chiara Balestra,^{1, 2, a)} Franz Kaiser,^{1, 3, b)} Debsankha Manik,^{4, c)} and Dirk Witthaut^{1, 3, d)}

¹⁾*Institute for Theoretical Physics, University of Cologne, Köln, 50937, Germany*

²⁾*Department of Mathematics "Giuseppe Peano", Università degli Studi di Torino, 10123 Torino, Italy*

³⁾*Forschungszentrum Jülich, Institute for Energy and Climate Research (IEK-STE), 52428 Jülich, Germany*

⁴⁾*Max Planck Institute for Dynamics and Self-Organization, Am Faßberg 17, 37077 Göttingen, Germany*

(Dated: 17 April 2022)

Networks of phase oscillators are studied in various contexts, in particular in the modeling of the electric power grid. A functional grid corresponds to a stable steady state, such that any bifurcation can have catastrophic consequences up to a blackout. But also the existence of multiple steady states is undesirable, as it can lead to sudden transitions or circulatory flows. Despite the enormous practical importance there is still no general theory of the existence and uniqueness of steady states in such systems. Analytic results are mostly limited to grids without Ohmic losses. In this article, we introduce a method to systematically construct the solutions of the real power load-flow equations in the presence of Ohmic losses and explicitly compute them for tree and ring networks. We investigate different mechanisms leading to multistability and discuss the impact of Ohmic losses on the existence of solutions.

The stable operation of the electric power grid relies on a precisely synchronized state of all generators and machines. All machines rotate at exactly the same frequency with fixed phase differences, leading to steady power flows throughout the grid. Whether such a steady state exists for a given network is of eminent practical importance. The loss of a steady state typically leads to power outages up to a complete blackout. But also the existence of multiple steady states is undesirable, as it can lead to sudden transitions, circulating flows and eventually also to power outages. Steady states are typically calculated numerically, but this approach gives only limited insight into the existence and (non-)uniqueness of steady states. Analytic results are available only for special network configuration, in particular for grids with negligible Ohmic losses or radial networks without any loops. In this article, we introduce a method to systematically construct the solutions of the real power load-flow equations in the presence of Ohmic losses. We calculate the steady states explicitly for elementary networks demonstrating different mechanisms leading to multistability. Our results also apply to models of coupled oscillators which are widely used in theoretical physics and mathematical biology.

I. INTRODUCTION

The electric power grid is one of the largest man-made systems, and a stably operating grid is integral for the entire economy, industry and almost all other technical infrastructures. The complexity of the power grid with thousands of generators, substations and transmission elements calls for an interdisciplinary approach to ensure stability in a transforming energy systems^{1,2}. In particular, the interrelation of structure and stability of complex grids has received widespread attention in recent years, see e.g.^{3–11}. These endeavours have been aided by the similarity of mathematical models across scientific disciplines. The fundamental models for power grid dynamics such as the classical model or the structure-preserving model^{12,13} are mathematically equivalent to the celebrated Kuramoto model with inertia^{14–17}. Therefore, results obtained on networks of Kuramoto oscillators can be easily translated to power grids and vice versa.

A central question across disciplines is whether a stable steady state exists and whether it is unique given a certain network structure. In the context of power grids, it is desirable to have a unique steady state. Grid operators strive to maintain the flows across each line below a certain limit to avoid disruptions. Ensuring this is much more difficult if one has to take into account multiple steady states, and hence multiple flow patterns across the lines. Analytic results have been obtained for various special cases. In particular, multistability has been ruled out for lossless grids in the two limiting cases of very densely connected networks^{14,18} as well as tree-like networks (very sparse)¹⁹. The existence of a steady state is determined by two factors: the distribution of the real power injections (natural frequencies for Kuramoto oscillators) and the strength of connecting lines. A variety of related results have also been obtained for tree-like

^{a)}Electronic mail: chiara.balestra@edu.unito.it

^{b)}Electronic mail: f.kaiser@fz-juelich.de

^{c)}Electronic mail: debsankha.manik@ds.mpg.de

^{d)}Electronic mail: d.witthaut@fz-juelich.de

distribution grids in power engineering, see e.g.²⁰.

The situation is more involved for networks of intermediate sparsity such as power transmission grids, which can give rise to multistability^{11,19,21–25}. The existence of multiple steady states in meshed networks can be traced back to the existence of *cycle flows*, which do not affect the power balance at any node in the grid. The number of and size of the cycles in the grid is thus an essential factor that determines the number of steady states¹⁹. Exploring the quantitative relationship between these topological factors and multistability, rigorous bounds on the number of steady states and mechanisms for a grid to switch from one steady state to another have been found^{11,19,23–27}.

Despite the great theoretical progress a general theory of the solvability of the power flow equations is still lacking. Most analytic studies focus on lossless grids^{7,9,11,19,21–26,28,29} or tree-like grids^{10,20,30–32}. Analytic results are extremely rare for the full power flow equations with ohmic losses in meshed networks^{21,33,34}.

In this article, we present a new approach to compute the steady states of the real power flow equations in general networks in the presence of ohmic losses, extending a prior study of lossless grids¹⁹. Our main contribution is a stepwise procedure to construct solutions. In a first step, flows and losses are treated as independent variables, turning the load flow equations into a linear set of equations. The inherent relations of flows and losses are reintroduced in a second step. Choosing an appropriate basis for the solution space of the linear set of equations, we can explicitly compute the coefficients leading to a consistent solution. Using this approach, we demonstrate that ohmic losses in general have two contrary effects on the solvability of the real power flow equations: On the one hand, increasing losses requires higher line capacities to be able to transport the same amount of power thereby potentially destabilizing the grid and thus losing stable fixed points. On the other hand, we show that high line losses may also cause multistability leading to additional stable fixed points through a mechanism non-existent for the lossless case.

The article is organized as follows. We first specify the mathematical structure of the problem and fix the notation in section II. We then briefly review the lossless case in section III to illustrate the fundamental importance of cycles and cycle flows. Section IV then constitutes the main part of the paper, introducing the stepwise approach. We then investigate two topologies in detail: a tree and a ring network, for which we lay down the procedures for computing all the steady states, in sections V and VI, respectively.

II. STEADY STATES IN POWER GRIDS AND OSCILLATOR NETWORKS

The load-flow equations constitute the fundamental model to describe the steady state of an AC power grid. The system state is defined in terms of the magnitude

and phase of the nodal voltages $V_j e^{i\theta_j}$, $j \in \{1, \dots, N\}$, which have to satisfy the energy conservation law. The nodes provide or consume a certain amount of real power P_j^{in} such that the real power balance reads

$$P_j^{\text{in}} = \sum_k b_{jk} V_j V_k \sin(\theta_j - \theta_k) + g_{jk} (V_j^2 - V_j V_k \cos(\theta_j - \theta_k)). \quad (1)$$

The variation of the voltage magnitudes V_j is intimately related with the provision and demand for reactive power. In general, generator nodes adapt the reactive power to fix the voltage to the reference level $V_j = V_{\text{ref}}$, while load nodes consume a fixed value of reactive power. The voltage magnitude V_j can depart from the reference level³⁵, but strict security rules are imposed to limit this voltage variation. In the present article we will focus on the real power balance equation (1) to explore the existence of solutions and possible routes to multistability. We neglect voltage variability to reduce the complexity of the problem and refer to^{9,10} for a detailed discussion of these issues. Technically, this corresponds to the assumption that the reactive power can be balanced at all nodes. Using appropriate units, referred to as the pu system in power engineering³⁶ we can thus set

$$V_j = V_{\text{ref}} = 1$$

for all nodes.

The network structure plays a decisive role for the existence and stability of steady states. This structure is encoded in the coupling coefficients b and g . For a given transmission line (j, k) with resistance r_{jk} and admittance x_{jk} we have

$$g_{jk} - ib_{jk} = \frac{1}{r_{jk} + ix_{jk}}, \quad (2)$$

where g_{jk} is the conductance of the line (j, k) , while the susceptance is given by $-b_{jk}$ (not $+b_{jk}$!). By this definition both g_{jk} and b_{jk} are generally positive for all transmission elements, with $g_{jk} = b_{jk} = 0$ if the two nodes j and k are not connected. In high voltage transmission grids, Ohmic losses are typically small such that g is small compared to b . In the limit of a lossless line, we obtain $g_{jk} = 0$ and $b_{jk} = 1/x_{jk} > 0$. In contrast, b and g are of similar magnitude in distribution grids.

A mathematically equivalent problem arises in the analysis of steady states of dynamical power system models. In particular, the dynamics of coupled synchronous machines is determined by the swing equation³⁷

$$I_j \frac{d^2 \theta_j}{dt^2} + D_j \frac{d\theta_j}{dt} = P_j^{\text{in}} - P_j^{\text{el}}, \quad (3)$$

whose steady states are again determined by Eq. (1). Furthermore, coupled oscillator models are used to describe the collective motion of various systems across scientific disciplines. For instance, the celebrated Kuramoto

model considers a set of N limit cycle oscillators whose state is described by their phases θ_j along the cycle. In many important applications^{38,39}, the equations of motions of the coupled system are given by

$$\frac{d\theta_j}{dt} = \omega_j + \sum_{k=1}^N K_{jk} \sin(\theta_k - \theta_j + \gamma_{jk}), \quad (4)$$

where ω_j is the intrinsic frequency of the j -th oscillator, $K_{jk} = K_{kj}$ is the coupling strength of oscillator j and k and $\gamma_{jk} = \gamma_{kj}$ is a phase shift. The fixed points of this model are determined by the algebraic equations $d\theta_j/dt = 0$, which, using basic trigonometric identities, are cast into the form

$$\begin{aligned} \omega_j + \sum_k K_{jk} \sin(\gamma_{jk}) &= \sum_k K_{jk} \cos(\gamma_{jk}) \sin(\theta_j^* - \theta_k^*) \\ &+ K_{jk} \sin(\gamma_{jk}) [1 - \cos(\theta_j^* - \theta_k^*)], \end{aligned} \quad (5)$$

where $\vec{\theta}^* = (\theta_1^*, \dots, \theta_N^*)$ is a fixed point. This equation is identical to the real power balance (1) if we identify $P_j^{\text{in}} = \omega_j + \sum_k K_{jk} \sin(\gamma_{jk})$, $b_{jk} = K_{jk} \cos(\gamma_{jk})$ and $g_{jk} = K_{jk} \sin(\gamma_{jk})$. We note that in the limit of a lossless line, $\gamma_{jk} = 0$ for all edges. In the following, we will fix a slack node s that can provide an infinite amount of power P_s which translates as an additional free parameter to the Kuramoto model given by the frequency at the node corresponding to the slack node ω_s . Therefore, different fixed points, i.e. solutions to Eq. 5, can have a different frequency at the slack node ω_s in this setup which differs from the way fixed points are typically considered in the Kuramoto model.

The stability of a given fixed point $\vec{\theta}^*$ is assessed using linear stability analysis by adding a small perturbation⁴⁰,

$$\theta_j = \theta_j^* + \xi_j, \quad j = 1, \dots, N. \quad (6)$$

For the first order model, the dynamics of the perturbations is to linear order given by

$$\frac{d\xi_j}{dt} = \sum_{k=1}^N w_{jk} (\xi_k - \xi_j)$$

with the weights

$$\begin{aligned} w_{jk} &= K_{jk} \cos(\theta_k^* - \theta_j^* + \gamma_{jk}) \\ &= b_{jk} \cos(\theta_k^* - \theta_j^*) + g_{jk} \sin(\theta_k^* - \theta_j^*). \end{aligned}$$

This relation is expressed in vectorial form as

$$\frac{d\vec{\xi}}{dt} = -\mathbf{A}\vec{\xi} \quad (7)$$

with the Laplacian-type matrix $\mathbf{A} \in \mathbb{R}^{N \times N}$ with elements

$$\Lambda_{jk} = \begin{cases} -w_{jk} & \text{for } j \neq k \\ \sum_{\ell} w_{j\ell} & \text{for } j = k. \end{cases} \quad (8)$$

Before we proceed we note that \mathbf{A} always has a zero eigenvalue corresponding to a global shift of all phases $\theta_j \rightarrow \theta_j + c$, which does not affect the synchronization of the system. We thus discard this mode and limit the stability analysis to the subspace perpendicular to it

$$\mathcal{D}_{\perp} = \{\vec{y} \in \mathbb{R}^N | (1, 1, \dots, 1)\vec{y} = 0\} \quad (9)$$

A steady state is linearly stable if all perturbations in \mathcal{D}_{\perp} are damped exponentially, which is the case if the real part of all eigenvalues of \mathbf{A} are strictly positive, i.e. if \mathbf{A} is positive definite on \mathcal{D}_{\perp} . We stress that this result also applies to the second order equation (3), cf.⁸.

Stability analysis becomes rather simple in the lossless case. Assuming that the network is connected and that the phase differences along any line are limited as

$$|\theta_k^* - \theta_j^*| < \frac{\pi}{2}, \quad (10)$$

the matrix \mathbf{A} is a proper graph Laplacian which is always positive definite on \mathcal{D}_{\perp} . Stable steady states that violate condition (10) do exist at the boundary of the stability region, but in most cases states with such large phase differences are unstable^{8,25,41}. Hence, we typically focus on states that do satisfy (10) and refer to this as the *normal operation* of the grid¹⁹.

The stability analysis is more involved in the presence of Ohmic losses, as \mathbf{A} is no longer symmetric. Hence, it rather corresponds to the Laplacian of a directed network, whose definiteness is harder to grasp analytically. In this case we will evaluate the linear stability of different steady states by direct numerical computations.

However, in the case where all off-diagonal elements of this matrix are strictly negative, we are able to gain limited analytical insight by the following Lemma:

Lemma 1. *Let $\vec{\theta}^* \in \mathbb{R}^N$ be an equilibrium of the Kuramoto model with phase lags as defined in Eq. 4. The equilibrium is linearly stable if all edges (j, k) have positive weights*

$$w_{jk} = K_{jk} \cos(\theta_k^* - \theta_j^* + \gamma_{jk}) > 0, \quad \forall (j, k).$$

Proof. The result can be proven by making use of Gershgorin's circle theorem⁴². Recall that the equilibrium is linearly stable if the Laplacian-type matrix \mathbf{A} is positive definite on \mathcal{D}_{\perp} , i.e. if all its eigenvalues have positive real part $\text{Re}(\mu_j) > 0, \forall j \in \{1, \dots, N-1\}$. According to Gershgorin's theorem, each eigenvalue μ_j is located in a disk in the complex plane with radius $R_j = \sum_{\ell \neq j} |\Lambda_{j,\ell}|$ centered at $\Lambda_{j,j}$. If the condition $w_{jk} > 0$ is satisfied, we have that $|\Lambda_{j,\ell}| = -\Lambda_{j,\ell}$. Therefore, applying Gershgorin's theorem results in the following inequality

$$\begin{aligned} |\mu_j - \Lambda_{j,j}| &\leq \sum_{\ell \neq j} |\Lambda_{j,\ell}| = -\sum_{\ell \neq j} \Lambda_{j,\ell}, \\ &= \Lambda_{j,j}. \end{aligned}$$

This inequality thus predicts that all eigenvalues μ_j have real part greater than or equal to zero $\text{Re}(\mu_j) \geq 0$.

Now it remains to show that the eigenvalue to the eigenvector $(1, 1, \dots, 1)^\top$ is the only zero eigenvalue. Assume that $\vec{v} \in \mathbb{R}^N$ is an eigenvector with eigenvalue $\mu = 0$. Assume that this vector has its minimum entry at position i , such that $v_i = \min(v_j)$, $j \in \{1, \dots, N\}$ and hence $v_i - v_j \leq 0$, $\forall j$. Then we arrive at

$$0 = (\mathbf{\Lambda} \vec{v})_i = \sum_{j \neq i} \Lambda_{ij} (v_i - v_j).$$

Since the off-diagonal elements Λ_{ij} are all negative by the assumption of the lemma, it follows that the entries of the vector at neighbouring nodes equal its minimum value $v_i = v_j$. We can now apply the same reasoning for next-nearest neighbours and proceed in the same way through the whole network to show that

$$v_i = v_j, \forall j \in \{1, \dots, N\},$$

which proves that $\vec{v} = (1, \dots, 1)^\top$ is the only eigenvector with vanishing eigenvalue $\mu = 0$. \square

III. THE LOSSLESS CASE

We briefly review the analysis of the lossless case to introduce the fundamentals of our approach as well as some notation and methodology. This review mostly follows¹⁹, but provides some additional examples and results.

A. Constructing solutions

In the lossless case, steady states are determined by

$$P_j = \sum_{k=1}^N b_{jk} \sin(\theta_j - \theta_k), \quad (11)$$

which has to be satisfied for every node $j \in \{1, \dots, N\}$. We obtain this by putting $g_{jk} = 0$ in (1), as well as assuming $V_j = V_{\text{ref}} = 1$. This is possible only if the power injections of the entire grid are balanced, i.e. $\sum_j P_j = 0$, which we assume henceforth. The main idea to construct all solutions of Eq. (11) is to shift the focus from nodal quantities to edges and cycles of the network.

To begin with, we introduce some notation. We label each edge in the network by a number $e = 1, \dots, M$ and summarize the line parameters in the diagonal matrix

$$\mathbf{B}_d = \text{diag}(b_1, \dots, b_M) \in \mathbb{R}^{M \times M}. \quad (12)$$

We then fix an orientation⁴³: for each edge e connecting nodes j and k , we arbitrarily choose k to be the “head” of the edge and j to be the “tail”, and refer to the edge as $e \hat{=} (j, k)$. Then we define the *flow* F_e on an edge $e \hat{=} (j, k)$ to be

$$F_e = b_e \sin(\theta_j - \theta_k). \quad (13)$$

If $F_e > 0$, the flow is directed from j to k and if $F_e < 0$ from k to j . Therefore F_e physically denotes the flow from the tail of the edge e to the head of e .

We then summarize all quantities in a vectorial form

$$\begin{aligned} \vec{P} &= (P_1, \dots, P_N)^\top \in \mathbb{R}^N, \\ \vec{\theta} &= (\theta_1, \dots, \theta_N)^\top \in \mathbb{R}^N, \\ \vec{F} &= (F_1, \dots, F_M)^\top \in \mathbb{R}^M. \end{aligned} \quad (14)$$

The topology of the network is encoded in the node-edge incidence matrix $\mathbf{I} \in \mathbb{R}^{N \times M}$ with elements⁴⁴

$$I_{j,e} = \begin{cases} +1 & \text{if node } j \text{ is the tail of edge } e \hat{=} (j, \ell), \\ -1 & \text{if node } j \text{ is the head of edge } e \hat{=} (j, \ell), \\ 0 & \text{otherwise.} \end{cases} \quad (15)$$

The relation between flows and phases (13) now becomes

$$\vec{F} = \mathbf{B}_d \sin(\mathbf{I}^\top \vec{\theta}), \quad (16)$$

where the sine function is taken element-wise, and Eq. (11) reads

$$\vec{P} = \mathbf{I} \vec{F}. \quad (17)$$

Now we can split the solution of (11) into two parts.

1. Construct all solutions of the linear set of equations (17) that respect the line limits $|F_e| \leq b_e$. As the matrix \mathbf{I} has the rank $N - 1$ ¹⁹, the solutions span a $M - N + 1$ dimensional subspace. Together with the line limits we typically have an $(M - N + 1)$ -dimensional polytope, or an empty set.
2. Out of all solution candidates \vec{F} in the polytope, find all vectors that can be expressed by phases $\vec{\theta}$ as in Eq. (16).

Fortunately, both steps can be operationalized in terms of the cycles of the network¹⁹. Let start constructing the solution space of Eq. (17). The kernel of the matrix \mathbf{I} corresponds exactly to *cycle flows*: A cycle flow being a constant flow along a cycle; with no in- or out-flow^{45–47}. The kernel has dimension $M - N + 1$, which reflects the fact that the cycles in a graph forms a vector space of dimension $M - N + 1$ ⁴⁸, a basis set of this space is called a fundamental cycle basis. This may be most easily interpreted for plane graphs (i.e. graphs drawn in a plane without any edge crossing), where we can simply choose the facets of the graph as fundamental cycles. A set of fundamental cycles \mathcal{B} is encoded in the corresponding cycle-edge incidence matrix $\mathbf{C}^B \in \mathbb{R}^{M \times (M - N + 1)}$ with elements

$$C_{e,c}^B = \begin{cases} +1 & \text{if the edge } e \text{ is part of the cycle } c \\ -1 & \text{if the reversed edge } e \text{ is part of cycle } c \\ 0 & \text{otherwise.} \end{cases} \quad (18)$$

Then all solutions of equation (17) can be written as

$$\vec{F} = \vec{F}^{(s)} + \mathbf{C}^B \vec{f}, \quad (19)$$

where $\vec{F}^{(s)} \in \mathbb{R}^M$ is a specific solution and $\vec{f} \in \mathbb{R}^{M-N+1}$ gives the strength of the cycle flows along each cycle in the chosen cycle basis.

Having obtained a flow vector \vec{F} , we can simply construct the associated phases as follows. Start at one particular node k (referred to as the slack node) and set $\theta_k = 0$. Then proceed to a neighbouring node j . Assuming that the connecting edge $e \triangleq (j, k)$ is oriented from node k to node j , the phase value reads

$$\theta_j = \theta_k + \Delta_e, \quad (20)$$

where the phase difference Δ_e is reconstructed from the flow F_e by inverting Eq. (13),

$$\begin{aligned} \Delta_e^+ &= \arcsin(F_e/b_e) \quad \text{or} \\ \Delta_e^- &= \pi - \arcsin(F_e/b_e). \end{aligned} \quad (21)$$

We can then proceed through the entire network to obtain all phases θ_j . For each edge e we have to decide whether we take the $+$ -solution or the $-$ -solution in Eq. (21). To keep track of this choice, we decompose the edge set of the network E into two parts,

$$\begin{aligned} E_+ &= \{e \in E | \Delta_e = \Delta_e^+\} \\ E_- &= \{e \in E | \Delta_e = \Delta_e^-\}, \end{aligned}$$

such that $E = E_+ \cup E_-$. For arbitrary flows \vec{F} however, this procedure will generally lead to inconsistencies, as most nodes can be reached from the slack via several different paths leading to different phases. The physically correct solutions are just the ones for which no inconsistencies occur. This is exactly the case if the sum of phase differences around an arbitrary cycle yields zero or an integer multiple of 2π . Fortunately, we have to check this condition only for the fundamental cycles as these provide a basis for the cycle space. For each of the fundamental cycles we define the winding number

$$\varpi_c = \frac{1}{2\pi} \sum_{e=1}^M C_{e,c}^B \Delta_e^\pm. \quad (22)$$

and we define the vector of winding numbers

$$\vec{\varpi} = (\varpi_1, \dots, \varpi_{M-N+1})^\top \in \mathbb{R}^{M-N+1}.$$

For a physical solution all these winding must be integer:

$$\varpi_c \in \mathbb{Z}$$

for some decomposition $E = E_+ \cup E_-$. It should be noted that the choice Δ_e^+ corresponds to the state of normal operation discussed in section II. Hence, states with $E_- = \emptyset$ are guaranteed to be stable, while states with $E_- \neq \emptyset$ are typically (but not always) unstable^{8,19,25}.

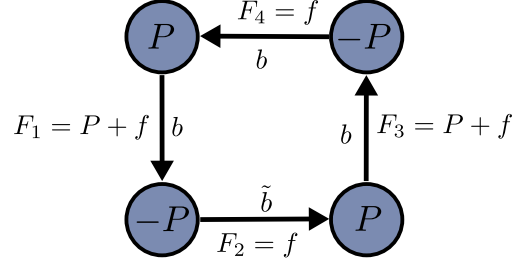


FIG. 1. Setup for the four node network used to demonstrate Braess' paradox for the lossless power flow. Four nodes (dark blue circles) with power injections P and $-P$ are connected via edges (black arrows) in a cyclic network. Arrows indicate the directions of real power flows F_1, F_2, F_3 and F_4 in the network and letters b and \tilde{b} represent the line susceptances of the adjacent transmission lines.

We have thus reformulated the problem of solving the nonlinear equation (11) to a two-stage procedure. This allows to systematically search for steady states and to quantify the number of steady states for a given network. In particular for plane networks the winding vector is unique, i.e. two steady states with same winding vector are identical¹⁹. We summarize these results in the following theorem.

Proposition 1. *Consider a connected lossless network with power injections $\vec{P} \in \mathbb{R}^N$. Then the following two statements are equivalent:*

1. $\vec{\theta}$ is a steady state, i.e., a real solution of equation (11).
2. The flows $\vec{F} \in \mathbb{R}^M$ satisfies the 'dynamic' conditions (17) with $|F_e| \leq b_e$ such that

$$\vec{F} = \vec{F}^{(s)} + \mathbf{C}^B \vec{f} \quad (23)$$

and the geometric condition (22)

$$\vec{\varpi}(\vec{f}) \in \mathbb{Z}^{M-N+1}. \quad (24)$$

for some decomposition $E = E_+ \cup E_-$.

B. Application: Braess' paradox

We demonstrate the applicability of the described approach for the elementary network depicted in Fig. 1. Two generators and two consumers are arranged on a cycle. All lines have the same strength b except for one with strength \tilde{b} . The general solution of the dynamic conditions (17) are given by

$$\vec{F} = \begin{pmatrix} F_1 \\ F_2 \\ F_3 \\ F_4 \end{pmatrix} = f \begin{pmatrix} 1 \\ 1 \\ 1 \\ 1 \end{pmatrix} + P \begin{pmatrix} 1 \\ 0 \\ 1 \\ 0 \end{pmatrix}, \quad (25)$$

and include one free parameter, the cycle flow strength f . Evaluating the line limits $|F_e| \leq b_e$ for all edges $e = 1, \dots, 4$ yields that f is restricted to the interval $f \in [f_{\min}, f_{\max}]$ with

$$f_{\min} = \max\{-b, -\tilde{b}\}, \quad f_{\max} = \min\{b - P, \tilde{b}\}.$$

To determine the physical value of the cycle flow strength f we then have to evaluate the geometric condition. We focus on the normal operation of the grid (i.e. $E_- = \emptyset$) such that the winding number reads

$$\varpi(f) = \frac{1}{2\pi} \left(2 \arcsin \left(\frac{f+P}{b} \right) + \arcsin \left(\frac{f}{b} \right) + \arcsin \left(\frac{f}{\tilde{b}} \right) \right).$$

For a small network with $N \leq 4$, a stable steady state can be found only for $\varpi(f) = 0$ ¹⁹. As $\varpi(f)$ is a monotonously increasing function of f , the condition for the existence of a stable steady state thus reads according to *Bolzano's theorem*

$$\varpi(f_{\min}) \leq 0 \quad \text{and} \quad \varpi(f_{\max}) \geq 0, \quad (26)$$

which is readily evaluated in terms of the system parameters.

Fig. 2 shows a stability map in terms of the line strength b and \tilde{b} . Obviously, a minimum connectivity is needed to transmit the real power from the generators to the consumers, which is formalized by the dynamic conditions. A solution of these conditions respecting the line limits can be found if

$$2b \geq P \quad \text{and} \quad b + \tilde{b} \geq P, \quad (27)$$

which is indicated by the yellow regions in the figure. In the light yellow areas, however, the solution of the dynamic condition lead to

$$\varpi(f_{\min}) > 0. \quad (28)$$

Hence, the geometric condition (26) cannot be satisfied and no normal steady state exists.

A remarkable effect is found for small values of b . An increase of the parameter \tilde{b} can take the system from the dark yellow to the light yellow parameter region such that the stable steady state is lost. Hence we find the surprising result that an increase of connectivity can impair the operation of a network up to a complete breakdown! This phenomenon can be seen as a manifestation of Braess' paradox first discussed in the context of traffic networks^{6,49–51}.

To obtain a deeper insight into this phenomenon, we can evaluate the geometric condition explicitly. For $\tilde{b} \geq b$ we find $f_{\min} = -b$ and the condition $\varpi(f_{\min}) \leq 0$ reads

$$2 \arcsin \left(\frac{P-b}{b} \right) + \arcsin(-1) + \arcsin \left(-\frac{b}{\tilde{b}} \right) \leq 0. \quad (29)$$

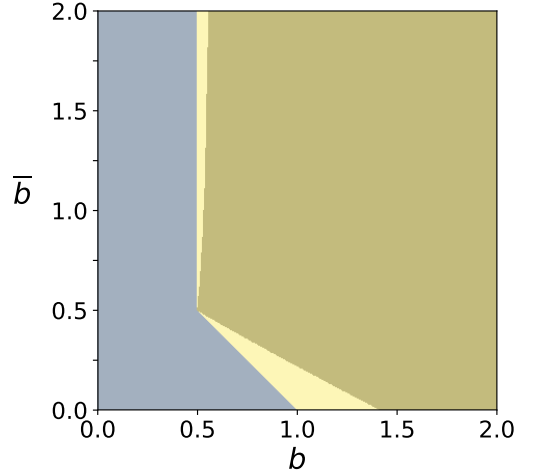


FIG. 2. Stability map in terms of the line strengths b and \tilde{b} in the four nodes cycle network sketched in figure 1 assuming $P = 1$ for simplicity. Normal stable steady states exist only if the line strengths are sufficiently large (dark yellow parameter region). No solutions exist in the grey area as the lines are too weak such that the dynamic conditions cannot be satisfied. Between these two parameter regions (light yellow area), all solutions of the dynamic conditions have $\varpi(f_{\min}) > 0$. Hence the geometric condition (26) cannot be satisfied and no normal steady state exists. A manifestation of Braess' paradox can be found if the line strength b is slightly above the critical value $b_c = 1/2$. A normal stable steady state exists for $\tilde{b} = 0.5$ (dark yellow area). But if the line strength \tilde{b} is increased, thus entering the light yellow area, this steady state gets lost and the grid becomes unstable.

Using several trigonometric identities, this condition is cast into the form

$$b \geq \frac{2P}{2 + \sqrt{2}} \quad \text{or} \quad \tilde{b} \leq \frac{b^3}{2(P-b)^2 - b^2}. \quad (30)$$

That is, if b is not too large, we find an *upper limit* for the connectivity \tilde{b} above which the steady state vanishes. However, for this limit tends to infinity as $b \geq \frac{2P}{2+\sqrt{2}}$ and Braess' paradox is no longer present.

IV. POWER GRIDS WITH OHMIC LOSSES

We now extend the approach introduced above to power grids with ohmic losses or oscillator networks with a general trigonometric coupling. The steady states are determined by the real power balance equation (cf. Eq. (1))

$$P_j = \sum_{k=1}^N b_{jk} \sin(\theta_j - \theta_k) + g_{jk} [1 - \cos(\theta_j - \theta_k)]. \quad (31)$$

Before we proceed to construct the solution to these equations we note an important difference to the lossless case.

The Ohmic losses occurring on the lines are not a priori known as they depend on the phases $\theta_1, \dots, \theta_N$. Hence the real power balance for the entire grid now reads

$$\sum_{j=1}^N P_j = P_{\text{losses}}(\theta_1, \dots, \theta_N). \quad (32)$$

Hence, for arbitrary P_1, \dots, P_N there will be typically no solution. This issue is solved by assuming that one of the nodes, referred to as the slack node, can provide an arbitrary amount of power to balance the losses. For the sake of consistency, we label the slack as $j = 1$ throughout this article and set $\theta_1 = 0$.

To solve the set of equations (31) for the remaining nodes $j \in \{2, \dots, N\}$ we decompose it into different parts as before and first formulate a linear system of equations. Before we start, we fix some notation and define the unsigned incidence matrix $\mathbf{E} \in \mathbb{R}^{N \times M}$ with elements $E_{je} = |I_{je}|$. For each edge $e \triangleq (j, k)$ we again define the flows by

$$F_e = b_e \sin(\theta_j - \theta_k)$$

and the losses by

$$L_e = g_e [1 - \cos(\theta_j - \theta_k)].$$

Using this notation, the power balance equations can be decomposed into three parts. First we have the dynamic condition, which now reads

$$(Ia) \quad P_j = \sum_{e=1}^M I_{je} F_e + E_{je} L_e, \quad \forall j \in \{2, \dots, N\}. \quad (33)$$

Flows and losses are limited by the line parameters such that we obtain the further conditions

$$(Ib) \quad \frac{F_e}{b_e} \in [-1, 1], \quad \frac{L_e}{g_e} \in [0, 2], \quad \forall e \in \{1, \dots, M\}. \quad (34)$$

In addition to that, flows and losses are not independent, but are both functions of the phase difference $\theta_j - \theta_k$. Using the trigonometric identity $\sin^2 + \cos^2 = 1$ we obtain the flow-loss condition

$$(II) \quad \left(\frac{F_e}{b_e}\right)^2 + \left(\frac{L_e}{g_e} - 1\right)^2 = 1, \quad \forall e \in \{1, \dots, M\}. \quad (35)$$

Finally, we have a geometric condition as in the lossless case

$$(III) \quad \varpi_c(F_1, \dots, L_1, \dots) = z \quad \text{with } z \in \mathbb{Z}, \quad \forall \text{ cycle } c. \quad (36)$$

In comparison to the lossless case we have M additional degrees of freedom L_1, \dots, L_M and M additional nonlinear conditions (35) to fix them. Furthermore, the knowledge of both F_e and L_e are necessary to fix the phases completely. Equation (21) is replaced by

$$\Delta_e = \begin{cases} \arcsin(F_e/b_e) & \text{if } L_e \leq g_e \\ \pi - \arcsin(F_e/b_e) & \text{if } L_e > g_e. \end{cases} \quad (37)$$

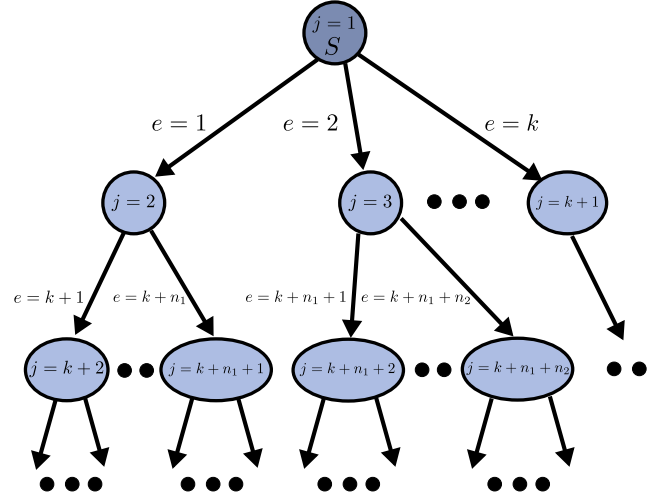


FIG. 3. Labeling of nodes (dark blue circles) and edges (black arrows) in a tree network used in Sec. V A. The slack node is taken as the root of the tree and labeled as $j = 1$ as indicated by the letter S and the darker blue colouring.

Still, there are two solution branches \pm per edge as in the lossless case, because the quadratic equation (35) has two solutions in general.

In conclusion, the general strategy to construct solutions consists of the following steps:

1. Find the solution space of the linear set of equations (33). We note that the addition of a cycle flows still does not affect the power balance, so the cycle flows remain basic degrees of freedom.
2. Use the flow-loss condition (35) to reduce the degrees of freedom of the system. In particular we will express all other degrees of freedom in terms of the cycle flow strength.
3. Finally, the cycle flows are fixed by the geometric conditions (36).

We now prove this approach by explicitly constructing the solutions for a tree network and a single cycle. We will show that including losses gives rise to additional mechanism of multistability.

V. TREE NETWORKS

We will first consider tree networks, i.e. networks without any closed cycles. Hence, we do not have to take into account the geometric condition (36) and concentrate on the solution of the flow-loss condition (35).

A. Fundamentals

We first introduce the basic notation, see Fig. 3. The slack node is taken as the root of the tree and labeled as $j = 1$. The remaining nodes are labeled according to the distance to the root: first nearest neighbors, then next-to-nearest neighbors, and so on. Every edge $e = 1, \dots, M = N - 1$ points to the node $e + 1$. For each node and edge, we must keep track of how it is connected to the root of the tree. We thus introduce the matrix $\mathbf{T} \in \mathbb{R}^{M \times M}$ by

$$T_{e,j} = \begin{cases} +1 & \text{if edge } e \text{ is on the path from node } \\ & j + 1 \text{ to the root} \\ 0 & \text{otherwise.} \end{cases}$$

Note that the labeling of the edges is chosen such that $T_{e,k}$ also indicates whether edge e is on the path from edge k to the root. Furthermore, we introduce the vectorial notation

$$\begin{aligned} \vec{F} &= (F_1, \dots, F_M)^\top, \\ \vec{L} &= (L_1, \dots, L_M)^\top, \\ \vec{x} &= (F_1, \dots, F_M, L_1, \dots, L_M)^\top. \end{aligned}$$

The dynamic condition (33) then reads

$$\vec{P} = \mathbf{I} \vec{x}, \quad (38)$$

where the matrix $\mathbf{I} \in \mathbb{R}^{(N-1) \times 2M}$ is obtained by concatenating the signed and unsigned incidence matrix $(\mathbf{I} | \mathbf{E})$ and removing the first line corresponding to the slack node. In particular, the matrix elements are given by

$$\mathcal{I}_{j-1,e} = \begin{cases} +1 & \text{if } e \leq M \text{ and } j \text{ is the tail of edge } \\ & e \text{ or if } e > M \text{ and } j \text{ is the tail or} \\ & \text{head of edge } e - M \\ -1 & \text{if } e \leq M \text{ and } j \text{ is the head of edge } \\ & e \\ 0 & \text{otherwise} \end{cases} \quad (39)$$

First, we need a specific solution $\vec{x}^{(s)}$ of the dynamic condition (38). For the sake of simplicity, we choose a solution with no losses, that is

$$\vec{x}^{(s)} = (\vec{F}_1^{(s)}, \dots, \vec{F}_M^{(s)}, 0, \dots, 0)^\top, \quad (40)$$

where

$$F_e^{(s)} = - \sum_{j=2}^N T_{e,j-1} P_j. \quad (41)$$

Then we have to construct the general solution to the dynamic conditions, i.e. we need a basis for the N -dimensional kernel of the matrix \mathbf{I} . The basis vectors are constructed such that they have losses only at one particular line, which yields

$$\begin{aligned} \vec{x}^{(e)} &= \begin{bmatrix} \vec{F}^{(e)} \\ \vec{L}^{(e)} \end{bmatrix}, \quad \forall e \in \{1, \dots, M\} \\ F_k^{(e)} &= 2T_{e,k} + \delta_{e,k} \\ L_k^{(e)} &= \delta_{e,k} \end{aligned}$$

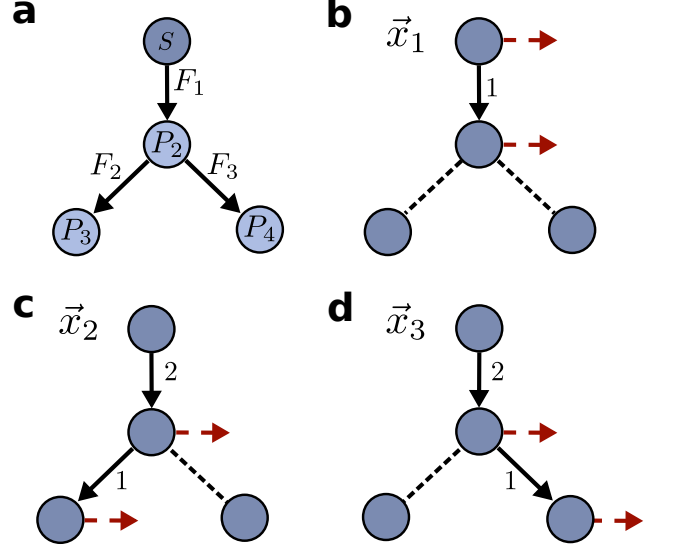


FIG. 4. (a) Simple tree network with $N = 4$ nodes $M = 3$ edges (a) Arrows indicate the orientation of edges which in turn determines the direction of flows. (b-d) Illustration of the basis vectors of the kernel of the matrix \mathbf{I} . The vectors $\vec{x}_e, e = 1, \dots, 3$ include losses at exactly one edge e , indicated by the dotted red arrows at the terminal nodes, and the flows needed to compensate this loss.

with the Kronecker symbol $\delta_{e,k}$. This set of basis vectors is illustrated in Fig. 4 for an elementary example. We note that these basis vectors are linearly independent as required, but not orthogonal. All solution candidates of the dynamic and the flow-loss conditions can be written as

$$\vec{x} = \vec{x}^{(s)} + \sum_{e=1}^M \alpha_e \vec{x}^{(e)}, \quad (42)$$

In terms of the flows and losses this yields

$$\begin{aligned} F_e &= F_e^{(s)} + 2 \sum_{k=e+1}^N T_{e,k} \alpha_k + \alpha_e, \\ L_e &= \alpha_e. \end{aligned} \quad (43)$$

To simplify the notation, we introduce the abbreviation

$$\mathcal{F}_e = - \sum_{j=2}^N T_{e,j-1} P_j + 2 \sum_{k=e+1}^N T_{e,k} \alpha_k, \quad (44)$$

which is the flow on the line e minus the losses,

$$\mathcal{F}_e = F_e - L_e = F_e - \alpha_e.$$

Now we can calculate the parameters α_e by substituting ansatz (43) into the flow-loss condition (35):

$$\left(\frac{\mathcal{F}_e + \alpha_e}{b_e} \right)^2 + \left(\frac{\alpha_e}{g_e} - 1 \right)^2 = 1. \quad (45)$$

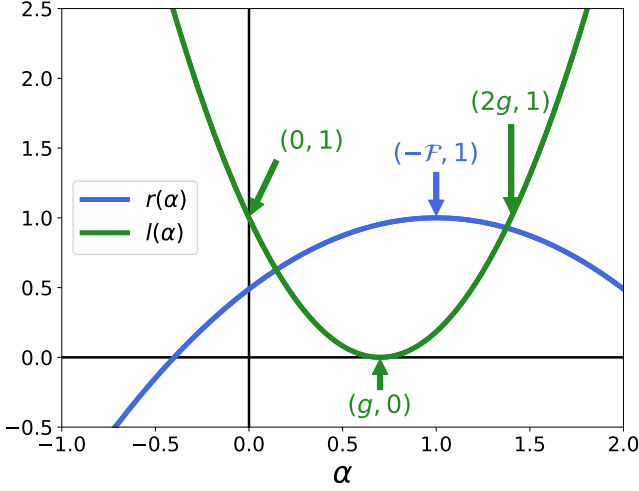


FIG. 5. Illustration of the two function $l(\alpha_e)$ and $r(\alpha_e)$ used in the proof of lemma 3 for arbitrary parameter values $g = 0.7$, $b = 1.4$ and $F = 1$.

To solve these quadratic equations we now have to proceed iteratively from $e = N - 1$ to $e = 1$ as the quantity \mathcal{F}_e depends on the solutions α_n of the lines $k = e + 1, \dots, N - 1$. We summarize our findings in the following lemma.

Lemma 2. *All potential solutions of the dynamic conditions and the load-flow condition for a tree network can be written as*

$$F_e = - \underbrace{\sum_{j=2}^N T_{e,j-1} P_j + 2 \sum_{k=e+1}^N T_{e,k} \alpha_k}_{=: \mathcal{F}_e} + \alpha_e$$

$$L_e = \alpha_e,$$

where the parameters α_e , $e \in \{M, M - 1, \dots, 1\}$ are determined iteratively as

$$\alpha_e^\pm = \frac{g_e b_e}{(g_e^2 + b_e^2)} \left[b_e - \frac{g_e}{b_e} \mathcal{F}_e - \sigma_e \sqrt{b_e^2 - \mathcal{F}_e^2 - 2g_e \mathcal{F}_e} \right], \quad (46)$$

where the sign $\sigma_e \in \{-1, +1\}$ indicates the solution branch. Hence, each potential solution is uniquely characterized by the sign vector $\vec{\sigma} = (\sigma_1, \dots, \sigma_M)^\top \in \{-1, +1\}^M$.

We note that this lemma does not yet tell us that a solution with parameters σ_e actually exists and is physically feasible. This is the case if and only if the resulting values for α_e^\pm are all real and positive and the line limits (34) are respected. Whether this is the case can be determined using the following lemma.

Lemma 3. *Equation (46) for the coefficients α_e^\pm has two real positive solutions which both satisfy the line limits*

(34) if and only if

$$b_e^2 \geq \mathcal{F}_e^2 + 2g_e \mathcal{F}_e. \quad (47)$$

The two solutions coalesce in the case of equality.

Proof. We first note that if condition (47) is satisfied, the discriminant in Eq. (46) is non-negative, such that all solutions are real. The two solutions coalesce if the discriminant vanishes, i.e. if $b_e^2 = \mathcal{F}_e^2 + 2g_e \mathcal{F}_e$.

We now have to show that the solution is positive and respects the line limits. To this end, we rewrite the flow-loss condition (35) as

$$\underbrace{\left(\frac{\alpha_e}{g_e} - 1 \right)^2}_{=: l(\alpha_e)} = 1 - \underbrace{\left(\frac{\alpha_e + \mathcal{F}_e}{b_e} \right)^2}_{=: r(\alpha_e)}. \quad (48)$$

The two parabola $l(\alpha_e)$ and $r(\alpha_e)$ are illustrated in Fig. 5. The left-hand side $l(\alpha_e)$ is non-negative everywhere with

$$\begin{aligned} l(\alpha_e) &\in [0, 1] && \text{if } \alpha_e \in [0, 2g_e] \\ l(\alpha_e) &> 1 && \text{if } \alpha_e \notin [0, 2g_e]. \end{aligned}$$

The right-hand side smaller or equal to one with

$$\begin{aligned} r(\alpha_e) &\in [0, 1] && \text{if } \alpha_e \in [-b_e - \mathcal{F}_e, +b_e - \mathcal{F}_e] \\ r(\alpha_e) &< 0 && \text{if } \alpha_e \notin [-b_e - \mathcal{F}_e, +b_e - \mathcal{F}_e]. \end{aligned}$$

Hence, we find the necessary condition for the crossing of the two parabola as

$$\begin{aligned} l(\alpha_e) &= r(\alpha_e) \in [0, 1], \\ L_e &= \alpha_e \in [0, 2g_e], \\ F_e &= \mathcal{F}_e + \alpha_e \in [-b_e, +b_e]. \end{aligned}$$

That is, if a solution α_e exists, it is guaranteed to be positive and satisfy the line limits. \square

We emphasize that condition (47) has to be satisfied for all edges $e \in \{1, \dots, M\}$, which again has to be verified iteratively.

B. Example

As an example we consider a grid with $N = 4$ nodes and $M = 3$ edges as depicted in Fig. 4 (a). The node-edge incidence matrix I and its modulus E will then be

$$I = \begin{bmatrix} +1 & 0 & 0 \\ -1 & +1 & +1 \\ 0 & -1 & 0 \\ 0 & 0 & -1 \end{bmatrix} \Rightarrow E = \begin{bmatrix} +1 & 0 & 0 \\ +1 & +1 & +1 \\ 0 & +1 & 0 \\ 0 & 0 & +1 \end{bmatrix}$$

and the tree matrix is given by

$$T = \begin{bmatrix} +1 & +1 & +1 \\ 0 & +1 & 0 \\ 0 & 0 & +1 \end{bmatrix}.$$

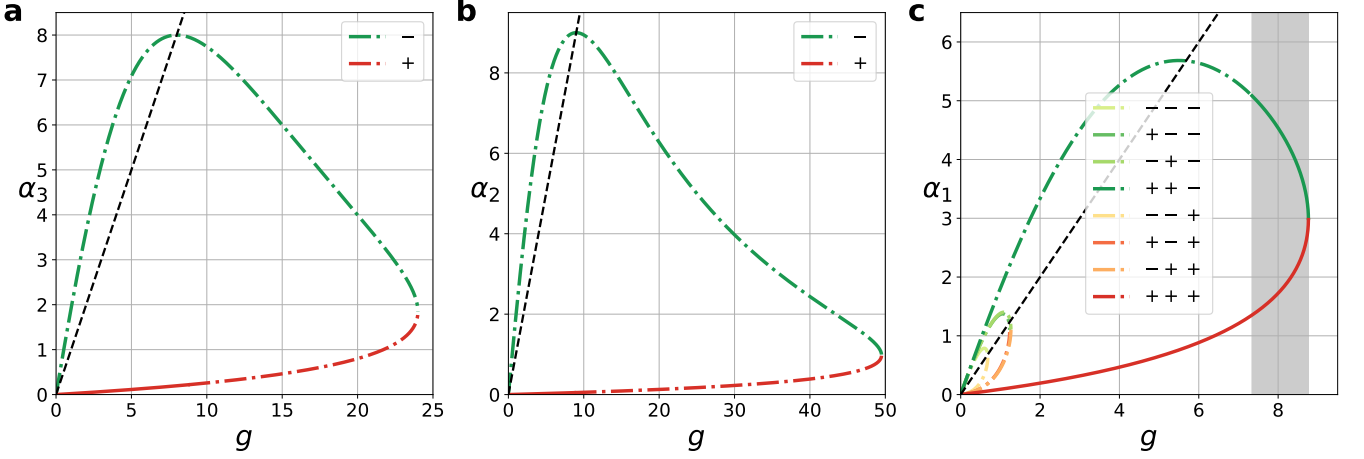


FIG. 6. Multiple solutions in a tree network with Ohmic losses. The possible values of the line losses α_e are shown as a function of the conductance g for the simple four node tree network shown in Fig. 4 and parameters $b = 10$, $P_2 = -1$, $P_3 = -1$ and $P_4 = -2$ for varying g as calculated according to Eq. (49). Solid, coloured lines indicate dynamically stable solutions and dotted, coloured lines indicate unstable ones. The black dotted line indicates points with $\alpha_i = g$ which determines which branch to choose when calculating angular differences according to Eq. (37). (a,b) Branching of α_2 and α_3 into two different solutions according to the different signs of the square root in the expression (49). (c) The solutions found for α_2 and α_3 can be used to subsequently calculate the solutions for α_1 . The solutions depend on the signs σ_e for all lines $e = 1, 2, 3$ such that we find 2^3 solution branches in total. The signs indicated in the legend are ordered as $(\sigma_3, \sigma_2, \sigma_1)$. In the region shaded in grey, there are two coexisting *stable* solutions.

The dynamic condition (33) thus reads

$$\begin{cases} P_2 = -F_1 + F_2 + F_3 + L_1 + L_2 + L_3 \\ P_3 = -F_2 - L_2 \\ P_4 = -F_3 - L_3 \end{cases}.$$

A particular solution of these equations is given by

$$\vec{x}^{(s)} = \begin{bmatrix} \vec{F}^{(s)} \\ \vec{L}^{(s)} \end{bmatrix} = (-P_2 - P_3 - P_4, -P_3, -P_4, 0, 0, 0)^\top.$$

and the kernel is spanned by the basis vectors

$$\begin{aligned} \vec{x}_1 &= (1, 0, 0, 1, 0, 0)^\top, \\ \vec{x}_2 &= (2, 1, 0, 0, 1, 0)^\top, \\ \vec{x}_3 &= (2, 0, 1, 0, 0, 1)^\top, \end{aligned}$$

which are illustrated in Fig. 4 (b-d). Hence, the general solution can be written as

$$\vec{x} = \begin{bmatrix} F_1 \\ F_2 \\ F_3 \\ L_1 \\ L_2 \\ L_3 \end{bmatrix} = \begin{bmatrix} F_1^{(s)} + 2\alpha_3 + 2\alpha_2 + \alpha_1 \\ F_2^{(s)} + \alpha_2 \\ F_3^{(s)} + \alpha_3 \\ \alpha_1 \\ \alpha_2 \\ \alpha_3 \end{bmatrix}.$$

The coefficients α_i , $i \in \{1, 2, 3\}$, are directly calculated in the order $e = 3, 2, 1$ via the formula

$$\alpha_e^\pm = \frac{g_e b_e}{(g_e^2 + b_e^2)} \left[b_e - \frac{g_e}{b_e} \mathcal{F}_e - \sigma_e \sqrt{b_e^2 - \mathcal{F}_e^2 - 2g_e \mathcal{F}_e} \right]. \quad (49)$$

with $\mathcal{F}_3 = F_3^{(s)}$, $\mathcal{F}_2 = F_2^{(s)}$ and $\mathcal{F}_1 = F_1^{(s)} + 2\alpha_2^\pm + 2\alpha_3^\pm$. We recall that in contrast to the cyclic case we do not have to consider the geometric condition. The values of α_e^\pm and hence also the flows and losses depend only on the signs $(\sigma_1, \sigma_2, \sigma_3)$ – and of course on the system parameters.

To explore the emergence of multistability in networks with Ohmic losses, we study the different solution branches as a function of the conductances g (6). For the sake of simplicity we assume that all lines have the same parameters, and keep both b and the power injections fixed.

In the lossless case $g = 0$, we trivially have $\alpha_e = 0$ for all edges and all solutions coalesce. For small values of g , the line losses α_e then increase approximately linearly and we find 2^3 different solutions in total, corresponding to the different choices of the signs $(\sigma_1, \sigma_2, \sigma_3)$. For each edge, the $+$ branch corresponds to a solution with low losses $L_e < g_e$ and the $-$ branch to a solution with high losses $L_e > g_e$. Nonlinear effects become important for higher values of g : The losses of the $+$ branches increase super-linearly, while the $-$ branches show a non-monotonic behaviour. For even higher values of g solutions vanish pairwise. The solution branches $\vec{\sigma} = (+, +, +)$ with the lowest overall losses and the branch $\vec{\sigma} = (+, +, -)$ vanishes last.

We further evaluate the dynamical stability for each solution branch by testing the definiteness of the matrix $\mathbf{\Lambda}$ defined in (8). The weights used in this Laplacian-type matrix can be rewritten directly in terms of the flows and losses. If nodes j and k are connected via edge

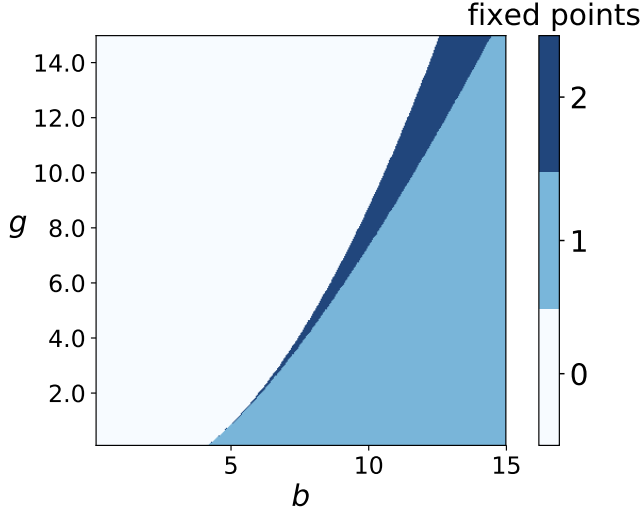


FIG. 7. Number of stable fixed points (colour code) of the lossy real power flow equations 1 for the four node tree network shown in Fig. 4,a with power injections $P_2 = -1$, $P_3 = -1$ and $P_4 = -2$ for varying line susceptance b (abscissa) and conductance g (ordinate). Whereas a minimum line capacity is required to result in any stable fixed points in the same way as for the lossless power flow, two effects that do not exist in the lossless case may be observed: Increasing conductances g and thus losses requires for higher line capacities b as expected. In addition to that, an additional stable fixed point arises for higher losses thus presenting a different mechanism for multistability.

e , we obtain

$$w_{jk} = \frac{b_e}{g_e}(g_e - L_e) \pm \frac{g_e}{b_e}F_e,$$

where the minus sign is chosen if j is the tail and k the head of edge e and the plus sign is chosen if k is the tail and j the head of edge e .

The results for the stability of the different solution branches are indicated by the dashing of the lines in figure 6 for the given network. We find that only the $(+++)$ -branch is stable for low losses. This is expected since in the lossless case there can be at most one stable solution¹⁹. The $(+++)$ -branch continuously merges into this stable solution in the limit $g \rightarrow 0$. More interestingly, also the $(++-)$ -branch becomes stable for large values of g . Hence, losses can stabilize fixed points.

A comprehensive analysis of the existence of solutions for the given sample network in terms of the grid parameters b and g is given in figure 7. Remarkably, the presence of Ohmic losses has two antithetic effects on the solvability of the real power load-flow equations. On the one hand, losses can prohibit the existence of solutions. Real power flows are generally higher in lossy networks as losses have to be balanced by additional flows. Hence, the minimum line strength b required for the existence of a solution increases with g . On the other hand, losses facilitate multistability. While the lossless equation can

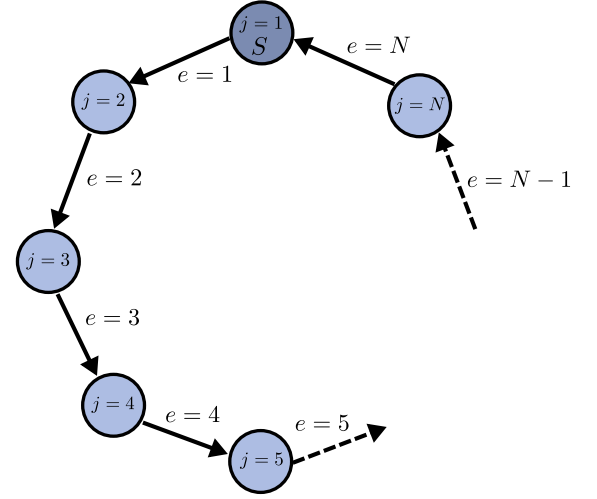


FIG. 8. Labeling of nodes (dark blue circles) and edges (black arrows) in a cyclic network used in Sec. VIA. The slack node is located at $j = 1$ and indicated here by the letter S and a colouring in darker blue.

have at most one stable fixed point for tree networks, two stable fixed points can exist if losses are added.

For example, for three consumer nodes with power injections $P_2 = -1, P_3 = -1$ and $P_4 = -2$, uniform line susceptances of $b = 10$ and $g = 8$, we find a dynamically stable solution branch with $\vec{\sigma} = (+, +, -)$ with flows $\vec{F} \approx (9.01, 1.04, 2.2)^\top$ and losses $\vec{L} \approx (4.54, 0.04, 0.2)^\top$ and another one with $\vec{\sigma} = (+, +, +)$ with flows $\vec{F} \approx (6.2, 1.04, 2.2)^\top$ and losses $\vec{L} \approx (1.73, 0.04, 0.2)^\top$. We recall that node 1 serves as a slack node. Hence, the power injection P_1 (or the natural frequency ω_1 in the oscillator context) is different for the two stable steady states.

VI. CYCLIC NETWORK

A. Fundamentals

We now consider a single closed cycle as depicted in figure 8. We label all nodes by $j \in \{1, \dots, N\}$ around the cycle in the mathematically positive direction starting at the slack node $j = 1$. Similarly, we label all lines $e \in \{1, \dots, N\}$ where line e corresponds to $(e, e + 1)$ and line $e = N$ corresponds to $(N, 1)$.

We now construct the solutions of the dynamic condition (38). As before, we choose a specific solution with no losses (cf. Eq. 40), where the flows satisfy

$$P_j = \sum_{e=1}^N I_{je} F_e^{(s)}, \quad \forall j \in \{2, \dots, N\}.$$

A solutions always exists, as the linear set of equations has rank $N - 1$. A proper initial guess can be obtained, for example, by solving the DC approximation³⁶.

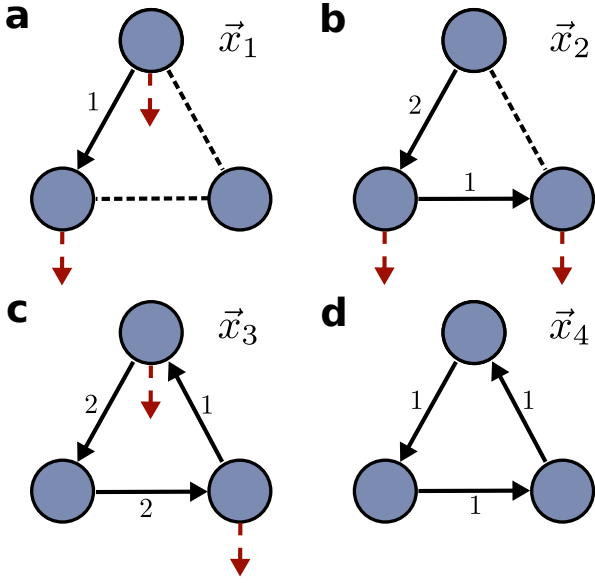


FIG. 9. Illustration of the basis vectors of the kernel of the matrix \mathcal{I} for a small cyclic network with $N = 3$ nodes. (a) The vectors $\vec{x}_e, e = 1, \dots, \vec{x}_N$ include losses at exactly one edge e , indicated by the dotted red arrows at the terminal nodes, and the flows needed to compensate this loss. (d) The basis vector \vec{x}_{N+1} represents a lossless cycle flow.

To construct the general solution, we further need a basis for the $(N + 1)$ -dimensional kernel of the matrix \mathcal{I} . As before we use a set of basis vectors that have losses only at one particular line,

$$\vec{x}^{(e)} = (\underbrace{2, \dots, 2}_{e-1 \text{ times}}, 1, \underbrace{0, \dots, 0}_{N-e \text{ times}}, \underbrace{0, \dots, 0}_{e-1 \text{ times}}, 1, \underbrace{0, \dots, 0}_{N-e \text{ times}})^\top. \quad (50)$$

In contrast to the tree network we need an additional basis vector describing a cycle flow

$$\vec{x}^{(N+1)} = (\underbrace{1, 1, \dots, 1}_{N \text{ times}}, 0, \dots, 0)^\top. \quad (51)$$

This set of basis vectors is illustrated in Fig. 9. All solution candidates of the dynamic and the flow-loss conditions can thus be written as

$$\vec{x} = \vec{x}^{(s)} + f \vec{x}^{(N+1)} + \sum_{e=1}^N \alpha_e \vec{x}^{(e)}, \quad (52)$$

where $f \in \mathbb{R}$ is a parameter giving the cycle flow strength. In terms of the flows and losses this yields

$$F_e = F_e^{(s)} + f + 2 \underbrace{\sum_{n=e+1}^N \alpha_n}_{=: \mathcal{F}_e} + \alpha_e, \quad (53)$$

$$L_e = \alpha_e.$$

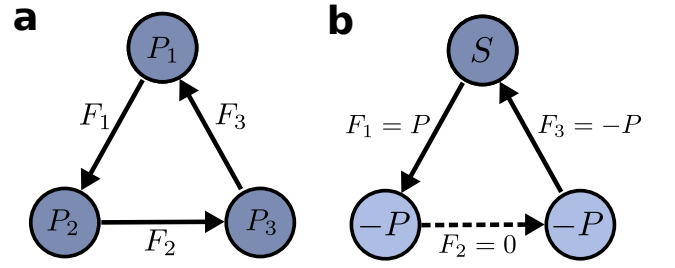


FIG. 10. Simple cycle network with three nodes (dark blue circles) and three edges (black arrows). (a) Arrows indicate the orientation of edges which in turn determines the direction of flows. We consider a network with power injections at the nodes P_1, P_2 and P_3 and power flows on the edges denoted F_1, F_2 and F_3 . (b) Example studied in section VIB. The node $j = 1$ is chosen as a slack node and the (indicated by symbol S) and the two other nodes are assumed to be consumer nodes with $P_{2,3} = -P$. Arrows again represent the edge orientations and the values give the specific solution $F_1^{(s)} = P, F_2^{(s)} = 0$ and $F_3^{(s)} = -P$.

As before, we can now calculate the parameters α_e iteratively from $e = N$ to $e = 1$ using the formula (cf. Eq. (46))

$$\alpha_e^\pm = \frac{g_e b_e}{(g_e^2 + b_e^2)} \left[b_e - \frac{g_e}{b_e} \mathcal{F}_e - \sigma_e \sqrt{b_e^2 - \mathcal{F}_e^2 - 2g_e \mathcal{F}_e} \right].$$

However, we now have to take into account that the quantities \mathcal{F}_e also depend on the parameter f – the cycle flow strength. Hence, each potential solution is now characterized by the continuous parameter f in addition to the signs $\sigma_1, \dots, \sigma_N \in \{-1, +1\}$. Whether a solution exists and respects the line limits can be determined from lemma 3, in particular from condition (47) which must be satisfied for all edges $e \in \{1, \dots, N\}$.

In a cyclic network we further have to satisfy the geometric condition (36), which fixes the remaining continuous degree of freedom f . For a single cycle, the winding number is given by

$$\varpi^{\vec{\sigma}} = \frac{1}{2\pi} \sum_{e=1}^M \Delta_e^{\sigma_e},$$

The phase differences $\Delta_e^{\sigma_e}$ and hence the winding number are determined by the line flows and losses via equation (37) and depend on the respective solution branch indicated by the signs $\vec{\sigma}$. Recall that the geometric condition states that the winding number ϖ can be an arbitrary integer. Hence there can be multiple solutions for f for a given set of signs $\sigma_1, \dots, \sigma_N$ if the cycle is large enough. This route to multistability was analyzed in detail for lossless networks in¹⁹.

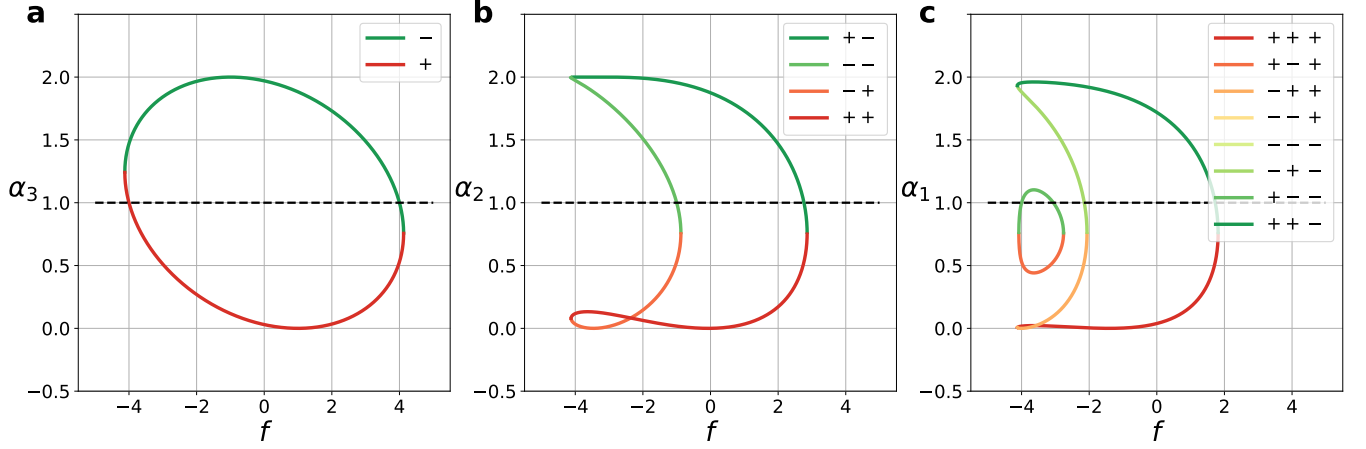


FIG. 11. The possible values of line losses $\alpha_{1,2,3}$ as a function of the cycle flow strength f for the simple three node cycle network shown in Fig. 10 and parameters $P = -1$, $g = 1$ and $b = 4$. Black dotted line indicates values where $\alpha_i = g$, thus determining the sign of angular differences according to eq.(37). (a) Branching of α_3 into two different solutions referred to as α_3^+ (dark red, bottom) and α_3^- (dark green, top) for the different signs of the square root as predicted by equation (55). (b-c) The solutions found for α_3 can be used to subsequently calculate the solutions for α_2 and then α_1 . The signs indicated here in the legend are ordered as (σ_3) , (σ_3, σ_2) and $(\sigma_3, \sigma_2, \sigma_1)$ for panels (a), (b) and (c), respectively.

B. Example

We analyze here a three-node cycle where node 1 is the slack node. The node-edge incidence matrix \mathbf{I} and its modulus \mathbf{E} will then be

$$\mathbf{I} = \begin{bmatrix} +1 & 0 & -1 \\ -1 & +1 & 0 \\ 0 & -1 & +1 \end{bmatrix} \Rightarrow \mathbf{E} = \begin{bmatrix} +1 & 0 & +1 \\ +1 & +1 & 0 \\ 0 & +1 & +1 \end{bmatrix}.$$

The dynamic condition (33) thus reads

$$\begin{cases} P_2 = F_2 - F_1 + L_1 + L_2 \\ P_3 = F_3 - F_2 + L_2 + L_3. \end{cases}$$

A particular solution of these equations is given by

$$\vec{x}^{(s)} = \begin{bmatrix} \vec{F}^{(s)} \\ \vec{L}^{(s)} \end{bmatrix} = (-P_2, 0, +P_3, 0, 0, 0)^\top.$$

and the kernel is spanned by the basis vectors

$$\begin{aligned} \vec{x}_1 &= (1, 0, 0, 1, 0, 0)^\top, \\ \vec{x}_2 &= (2, 1, 0, 0, 1, 0)^\top, \\ \vec{x}_3 &= (2, 2, 1, 0, 0, 1)^\top, \\ \vec{x}_4 &= (1, 1, 1, 0, 0, 0)^\top, \end{aligned}$$

which are illustrated in Fig. 9. Hence, the general solution can be written as

$$\vec{x} = \begin{bmatrix} F_1 \\ F_2 \\ F_3 \\ L_1 \\ L_2 \\ L_3 \end{bmatrix} = \begin{bmatrix} F_1^{(s)} + f + 2\alpha_3 + 2\alpha_2 + \alpha_1 \\ F_2^{(s)} + f + 2\alpha_3 + \alpha_2 \\ F_3^{(s)} + f + \alpha_3 \\ \alpha_1 \\ \alpha_2 \\ \alpha_3 \end{bmatrix}. \quad (54)$$

The coefficients $\alpha_{1,2,3}$ are calculated as a function of f iteratively starting from $N = 3$ via the formula

$$\alpha_e^\pm = \frac{g_e b_e}{(g_e^2 + b_e^2)} \left[b_e - \frac{g_e}{b_e} \mathcal{F}_e \pm \sqrt{b_e^2 - \mathcal{F}_e^2 - 2g_e \mathcal{F}_e} \right], \quad (55)$$

with $\mathcal{F}_3 = F_e^{(s)} + f$, $\mathcal{F}_2 = F_e^{(s)} + f + 2\alpha_3^\pm$ and $\mathcal{F}_1 = F_e^{(s)} + f + 2\alpha_2^\pm + 2\alpha_3^\pm$. The results are shown in Fig. 11(a-c) for all different possibilities of the sign vector $(\sigma_1, \sigma_2, \sigma_3)$: for α_3 we have 2 choices, then for α_2 we have $2^2 = 4$ choices (two choices for each of α_2 and α_3) and finally we have $2^3 = 8$ choices for α_1 . For the sake of simplicity, we have chosen $P_2 = P_3 = 1$ in this example. Notably, all branches of the solutions must form closed curves when plotted via the parameter f . This is due to the fact that a real solution of the equation (49) can only vanish when the discriminant goes to zero, i.e. when it collides with another branch of the solution.

The remaining parameter f is determined by the geometric condition (36). To evaluate this condition and to finally determine all steady states we plot the winding number

$$\varpi^{\vec{\sigma}}(f) = \frac{1}{2\pi} \sum_{e=1}^M \Delta_e$$

as a function of f in Fig. 12. The phase differences are given by (cf. Eq. (37)).

$$\Delta_e^{\sigma_e} = \begin{cases} \arcsin(F_e/b_e) & \text{if } L_e \leq g_e \\ \pi - \arcsin(F_e/b_e) & \text{if } L_e > g_e. \end{cases}$$

They depend on the solution branch, i.e. on the values of the σ_e and so does the winding number. For the given

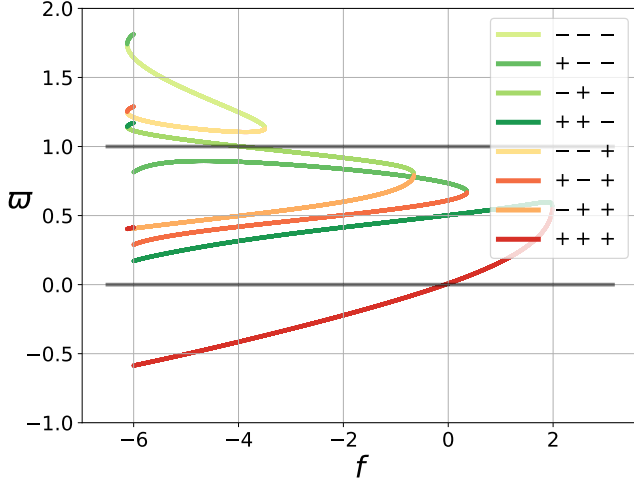


FIG. 12. The winding number ϖ as a function of the cycle flow strength f for different solution branches in the three node network depicted in Fig. 10. Solutions require that $\varpi \in \mathbb{Z}$, cf. Eq. (36). Colour code as in Fig. 11,c for all panels.

cyclic network we find 2^3 solution branches, which have to be considered when evaluating the geometric condition, see Fig. 12. Inspecting the winding number $\varpi^{\vec{\sigma}}(f)$ for each branch, we find 2 steady states, of which one is stable and one is unstable. Again, the stable fixed point is given by the $(+, +, +)$ -branch which has the lowest Ohmic losses.

However, we can find two dynamically stable branches for higher losses as in the case for the tree network. For example, fixing line susceptances and conductances $b = g = 3$ and power injections $P_2 = P_3 = -1$, we find again two dynamically stable branches corresponding to low losses $\vec{\sigma} = (+, +, +)$ and high losses $\vec{\sigma} = (+, +, -)$.

VII. SUMMARY AND DISCUSSION

In this article, we studied solutions to the real power load-flow equations in AC transmission grids of general topology with a special focus on the impact of Ohmic losses. Extending our previous work¹⁹, we constructed an analytical method for computing all load flow solutions, both stable and unstable ones. We demonstrated how to explicitly compute all steady states in two elementary test topologies: a 4-node tree and a 3-node ring.

We find that analogous to the lossless case, different solutions exist corresponding to different winding numbers (22) along each basis cycle, as well as a choice between two solution branches in each edge. The two branches correspond to a state with low losses and phase differences on the respective edge (+ branch) and high losses and phase difference (− branch).

We show that ohmic losses have two conflicting effects on the existence and number of steady states. On the one hand, high losses must be compensated by higher flows.

Hence, solutions may vanish due to ohmic losses unless the line capacities are also increased. On the other hand, ohmic losses can stabilize certain solution branches and thus foster multistability. In particular, we demonstrate that two grid topologies that have been proven to exhibit *no* multistability in the lossless case – trees and 3-node rings – *are* multistable in the lossy case for certain parameter values.

ACKNOWLEDGMENTS

We thank Tom Brown and Johannes Schiffer for valuable discussions. We gratefully acknowledge support from the German Federal Ministry of Education and Research (grant no. 03EK3055B) and the Helmholtz Association (via the joint initiative “Energy System 2050 – A Contribution of the Research Field Energy” and the grant no. VH-NG-1025). D.M. acknowledges funding from the Max Planck Society.

- ¹C. D. Brummitt, P. D. Hines, I. Dobson, C. Moore, and R. M. D’Souza, “Transdisciplinary electric power grid science,” *Proceedings of the National Academy of Sciences* **110**, 12159–12159 (2013).
- ²M. Timme, L. Kocarev, and D. Witthaut, “Focus on networks, energy and the economy,” *New journal of physics* **17**, 110201 (2015).
- ³G. Filatrella, A. H. Nielsen, and N. F. Pedersen, “Analysis of a power grid using a kuramoto-like model,” *The European Physical Journal B* **61**, 485–491 (2008).
- ⁴D. Witthaut and M. Timme, “Braess’s paradox in oscillator networks, desynchronization and power outage,” *New journal of physics* **14**, 083036 (2012).
- ⁵F. Dörfler and F. Bullo, “Synchronization and transient stability in power networks and nonuniform kuramoto oscillators,” *SIAM Journal on Control and Optimization* **50**, 1616–1642 (2012).
- ⁶D. Witthaut and M. Timme, “Nonlocal failures in complex supply networks by single link additions,” *The European Physical Journal B* **86**, 377 (2013).
- ⁷F. Dörfler, M. Chertkov, and F. Bullo, “Synchronization in complex oscillator networks and smart grids,” *Proceedings of the National Academy of Sciences* **110**, 2005–2010 (2013).
- ⁸D. Manik, D. Witthaut, B. Schäfer, M. Matthiae, A. Sorge, M. Rohden, E. Katifori, and M. Timme, “Supply networks: Instabilities without overload,” *The European Physical Journal Special Topics* **223**, 2527–2547 (2014).
- ⁹J. W. Simpson-Porco, “A theory of solvability for lossless power flow equations—part i: Fixed-point power flow,” *IEEE Transactions on Control of Network Systems* **5**, 1361–1372 (2017).
- ¹⁰J. W. Simpson-Porco, “A theory of solvability for lossless power flow equations—part ii: Conditions for radial networks,” *IEEE Transactions on Control of Network Systems* **5**, 1373–1385 (2017).
- ¹¹S. Jafarpour, E. Y. Huang, K. D. Smith, and F. Bullo, “Multistable synchronous power flows: From geometry to analysis and computation,” *arXiv preprint arXiv:1901.11189* (2019).
- ¹²P. M. Anderson and A. A. Fouad, *Power system control and stability* (John Wiley & Sons, 2008).
- ¹³A. R. Bergen and D. J. Hill, “A structure preserving model for power system stability analysis,” *IEEE Transactions on Power Apparatus and Systems*, 25–35 (1981).
- ¹⁴Y. Kuramoto, “International symposium on mathematical problems in theoretical physics,” *Lecture notes in Physics* **30**, 420 (1975).

- ¹⁵S. H. Strogatz, "From kuramoto to crawford: exploring the onset of synchronization in populations of coupled oscillators," *Physica D: Nonlinear Phenomena* **143**, 1–20 (2000).
- ¹⁶J. A. Acebrón, L. L. Bonilla, C. J. P. Vicente, F. Ritort, and R. Spigler, "The kuramoto model: A simple paradigm for synchronization phenomena," *Reviews of modern physics* **77**, 137 (2005).
- ¹⁷A. Arenas, A. Díaz-Guilera, J. Kurths, Y. Moreno, and C. Zhou, "Synchronization in complex networks," *Physics reports* **469**, 93–153 (2008).
- ¹⁸R. Taylor, "There is no non-zero stable fixed point for dense networks in the homogeneous kuramoto model," *Journal of Physics A: Mathematical and Theoretical* **45**, 055102 (2012).
- ¹⁹D. Manik, M. Timme, and D. Witthaut, "Cycle flows and multistability in oscillatory networks," *Chaos: An Interdisciplinary Journal of Nonlinear Science* **27**, 083123 (2017).
- ²⁰H.-D. Chiang and M. E. Baran, "On the existence and uniqueness of load flow solution for radial distribution power networks," *IEEE Transactions on Circuits and Systems* **37**, 410–416 (1990).
- ²¹A. J. Korsak, "On the question of uniqueness of stable load-flow solutions," *IEEE Transactions on Power Apparatus and Systems*, 1093–1100 (1972).
- ²²D. A. Wiley, S. H. Strogatz, and M. Girvan, "The size of the sync basin," *Chaos: An Interdisciplinary Journal of Nonlinear Science* **16**, 015103 (2006).
- ²³J. Ochab and P. Gora, "Synchronization of coupled oscillators in a local one-dimensional kuramoto model," *Acta Physica Polonica. Series B, Proceedings Supplement* **3**, 453–462 (2010).
- ²⁴R. Delabays, T. Coletta, and P. Jacquod, "Multistability of phase-locking and topological winding numbers in locally coupled kuramoto models on single-loop networks," *Journal of Mathematical Physics* **57**, 032701 (2016).
- ²⁵R. Delabays, T. Coletta, and P. Jacquod, "Multistability of phase-locking in equal-frequency kuramoto models on planar graphs," *Journal of Mathematical Physics* **58**, 032703 (2017).
- ²⁶D. Mehta, N. S. Daleo, F. Dörfler, and J. D. Hauenstein, "Algebraic geometrization of the kuramoto model: Equilibria and stability analysis," *Chaos: An Interdisciplinary Journal of Nonlinear Science* **25**, 053103 (2015).
- ²⁷T. Coletta, R. Delabays, I. Adagideli, and P. Jacquod, "Topologically protected loop flows in high voltage ac power grids," *New Journal of Physics* **18**, 103042 (2016).
- ²⁸S. Park, R. Zhang, J. Lavaei, and R. Baldick, "Monotonicity between phase angles and power flow and its implications for the uniqueness of solutions," in *Proceedings of the 52nd Hawaii International Conference on System Sciences* (2019).
- ²⁹A. Zachariah, Z. Charles, N. Boston, and B. Lesieutre, "Distributions of the number of solutions to the network power flow equations," in *2018 IEEE International Symposium on Circuits and Systems (ISCAS)* (IEEE, 2018) pp. 1–5.
- ³⁰K. N. Miu and H.-D. Chiang, "Existence, uniqueness, and monotonic properties of the feasible power flow solution for radial three-phase distribution networks," *IEEE Transactions on Circuits and Systems I: Fundamental Theory and Applications* **47**, 1502–1514 (2000).
- ³¹J. Lavaei, D. Tse, and B. Zhang, "Geometry of power flows in tree networks," in *2012 IEEE Power and Energy Society General Meeting* (IEEE, 2012) pp. 1–8.
- ³²S. Bolognani and S. Zampieri, "On the existence and linear approximation of the power flow solution in power distribution networks," *IEEE Transactions on Power Systems* **31**, 163–172 (2015).
- ³³W. A. Bukhsh, A. Grothey, K. I. McKinnon, and P. A. Trodden, "Local solutions of the optimal power flow problem," *IEEE Transactions on Power Systems* **28**, 4780–4788 (2013).
- ³⁴B. Cui and X. A. Sun, "Solvability of power flow equations through existence and uniqueness of complex fixed point," *arXiv preprint arXiv:1904.08855* (2019).
- ³⁵J. W. Simpson-Porco, F. Dörfler, and F. Bullo, "Voltage collapse in complex power grids," *Nature communications* **7**, 10790 (2016).
- ³⁶A. J. Wood, B. F. Wollenberg, and G. B. Sheblé, *Power generation, operation, and control* (John Wiley & Sons, 2013).
- ³⁷T. Nishikawa and A. E. Motter, "Comparative analysis of existing models for power-grid synchronization," *New Journal of Physics* **17**, 015012 (2015).
- ³⁸H. Daido, "Quasientrainment and slow relaxation in a population of oscillators with random and frustrated interactions," *Physical review letters* **68**, 1073 (1992).
- ³⁹D. M. Abrams, R. Mirollo, S. H. Strogatz, and D. A. Wiley, "Solvable model for chimera states of coupled oscillators," *Physical review letters* **101**, 084103 (2008).
- ⁴⁰S. H. Strogatz, *Nonlinear Dynamics and Chaos with Student Solutions Manual: With Applications to Physics, Biology, Chemistry, and Engineering* (CRC Press, 2018).
- ⁴¹W. Chen, J. Liu, Y. Chen, S. Z. Khong, D. Wang, T. Başar, L. Qiu, and K. H. Johansson, "Characterizing the positive semidefiniteness of signed laplacians via effective resistances," in *2016 IEEE 55th Conference on Decision and Control (CDC)* (IEEE, 2016) pp. 985–990.
- ⁴²S. A. Gershgorin, "Über die abgrenzung der eigenwerte einer matrix," *Izvestiya Rossiiskoi Akademii Nauk, Seriya Matematicheskaya*, 749–754 (1931).
- ⁴³C. Godsil and G. F. Royle, *Algebraic graph theory*, Vol. 207 (Springer Science & Business Media, 2013).
- ⁴⁴M. E. J. Newman, *Networks: an introduction* (Oxford University Press, 2010).
- ⁴⁵H. Ronellenfitsch, M. Timme, and D. Witthaut, "A dual method for computing power transfer distribution factors," *IEEE Transactions on Power Systems* **32**, 1007–1015 (2016).
- ⁴⁶H. Ronellenfitsch, D. Manik, J. Hörsch, T. Brown, and D. Witthaut, "Dual theory of transmission line outages," *IEEE Transactions on Power Systems* **32**, 4060–4068 (2017).
- ⁴⁷J. Hörsch, H. Ronellenfitsch, D. Witthaut, and T. Brown, "Linear optimal power flow using cycle flows," *Electric Power Systems Research* **158**, 126–135 (2018).
- ⁴⁸R. Diestel, *Graph Theory* (Springer, New York, 2010).
- ⁴⁹D. Braess, "Über ein paradoxon aus der verkehrsplanung," *Unternehmensforschung* **12**, 258–268 (1968).
- ⁵⁰T. Coletta and P. Jacquod, "Linear stability and the braess paradox in coupled-oscillator networks and electric power grids," *Physical Review E* **93**, 032222 (2016).
- ⁵¹E. B. T. Tchuisseu, D. Gomila, P. Colet, D. Witthaut, M. Timme, and B. Schäfer, "Curing braess' paradox by secondary control in power grids," *New Journal of Physics* **20**, 083005 (2018).